Active Front Steering-Based Electronic Stability Control for Steer-by-Wire Vehicles via Terminal Sliding Mode and Extreme Learning Machine

Jie Zhang, Hai Wang, *Senior Member, IEEE*, Mingyao Ma, *Member, IEEE*, Ming Yu, Amirmehdi Yazdani, *Member, IEEE*, and Long Chen

***Abstract*—In this article, a novel active front steering (AFS) control strategy including the upper controller and the lower controller is proposed to improve the yaw stability and maneuverability for steer-by-wire (SbW) vehicles. The adaptive recursive integral terminal sliding mode (ARITSM) control is adopted in the upper controller for guaranteeing the convergence performance of both the actual sideslip angle and the yaw rate with strong robustness and fast convergence rate. Then, a fast nonsingular terminal sliding mode (FNTSM) control with extreme learning machine (ELM) estimator to estimate its equivalent control is designed in the lower controller to track the desired front wheel steering angle calculated from the upper controller for driving the sideslip angle and the yaw rate to converge ideal value. It is shown that the upper controller takes two controlled variables (vehicle sideslip angle and yaw rate) and only one control input (front steering angle) into consideration, which can obtain a better performance compared with the case of using only one of these values. Since using the ELM technique in the lower controller to estimate the equivalent control of the FNTSM, not only the dependence of SbW system dynamics can be alleviated in the process of designing controller but also the excellent steering control performance can be achieved. Comparative simulations are carried out by utilizing Carsim and Matlab software to validate the excellent performance of the proposed control strategy for different steering maneuvers.**

***Index Terms*—Active front steering, electronic stability control, extreme learning machine (ELM), terminal sliding mode, steer-by-wire (SbW) vehicles.**

I. Introduction

ALTHOUGH the rapid development of the automotive industry has brought great convenience to our daily life, the number of deaths caused by traffic accidents is increasing every year with the complexity of vehicle driving conditions [1]. In order to improve the vehicle safety factor and driving performance, numerous studies have been conducted for the vehicle yaw stability control [2]. Electronic stability control (ESC) is the most effective systems, which includes active front-steering (AFS) control system, anti-lock braking system (ABS) and direct yaw-moment control (DYC) system [3].

Although the ESC schemes based on ABS designed in [4]–[7] can enhance the vehicle stability, there still exists some problems. For example, ABS-based ESC can only guarantee the vehicle stability in low-speed scenarios, which may lead to worse driving feelings and severe driving situation due to the sudden reduction of vehicle speed caused by the braking force. In [8], a fuzzy logic DYC control system was proposed to improve the yaw stability of the all-wheel-drive electric vehicles. An adaptive neural network sliding mode controller was designed based on the system uncertainty approximation to obtain superior stability and tracking performance at different driving conditions [9]. In order to solve the problems of collision avoidance and stabilization for vehicles in emergency steering situation, a novel emergency steering control strategy was developed based on hierarchical control architecture [10].

In recent years, since the yaw stability of vehicles can be guaranteed by applying the AFS control system, which has attracted much attention among researchers. In [11], a robust sliding mode control (SMC) was designed for four wheel active steering (4WAS) vehicle. Some researchers and automotive engineers are devoted to designing the controller integrated with the AFS and DYC, which exhibits the excellent trade-off between the control performance and the design complexity. For instance, a generalized proportional–integral (PI) control law was proposed to guarantee the vehicle stability through AFS/DYC [12]. In [13], a new coordination scheme based on optimal guaranteed cost control technique was proposed by coordinating AFS and DYC to track the system reference. In [14], a new Takagi-Sugeno (T-S) fuzzy based SMC strategy was presented for the AFS system to improve the cornering stability of vehicles. Then, in [15], a dynamic game theory as a general framework was proposed to enable the AFS and active rear steering (ARS) systems to work together for providing more stability for vehicle path tracking control. In [16], a random projection neural network-based adaptive neural control method was proposed to further enhance the vehicle yaw stability with AFS system,

Manuscript received June 9, 2020; revised September 22, 2020; accepted November 3, 2020. Date of publication November 6, 2020; date of current version January 22, 2021. This work was supported by the National Nature Science Funds of China under Grants 61771178 and 51977054. The review of this article was coordinated by Dr. S. Anwar. *(Corresponding author: Hai Wang.)*

Jie Zhang, Mingyao Ma, and Ming Yu are with the School of Electrical and Automation Engineering, Hefei University of Technology, Hefei 230009, China (e-mail: zhangjie@mail.hfut.edu.cn; miyama@hfut.edu.cn; mltrym@163.com).

Hai Wang and Amirmehdi Yazdani are with the Discipline of Engineering and Energy, and Centre for Water-Energy-Waste, Murdoch University, Perth, WA 6150, Australia (e-mail: hai.wang@murdoch.edu.au; amirmehdi.yazdani@murdoch.edu.au).

Long Chen is with the College of Electronic Information, Hangzhou Dianzi University, Hangzhou 310018, China (e-mail: chenlong@hdu.edu.cn).

Digital Object Identifier 10.1109/TVT.2020.3036400

including tracking desired yaw rate, sideslip angle and intended path.

For the purpose of improving the yaw stability and maneuverability of the intelligent vehicle, steer-by-wire (SbW) system as a new steering technology has recently attracted many researches' attention, and SbW-based AFS control have been proposed to achieve the control purpose. In [17] and [18], yaw stability control strategies based on the estimated sideslip angle by a linear observer and integral terminal sliding mode control (ITSMC) were designed for SbW-based AFS, but only the yaw rate was considered in the process of controller design. In order to make the sideslip angle and the yaw rate converge to their desired values, an adaptive controller with observer to identity sideslip angle and cornering stiffness was presented in [19], which can obtain better control performance than the case that only considers one of them.

In order to track the desired front wheel steering angle being the control input of the AFS and the reference signal of the SbW system, a number of advanced control techniques have been proposed. In [20] and [21], the conventional proportional–derivative (PD) control technique and the state feedback control scheme were proposed to drive the steering angle respectively. The SMC technique was employed in the SbW system successfully with the results that the excellent steering performance against parameter uncertainties and road condition changes were achieved in [22]–[25]. However, SbW system parameter and disturbance information should be required in designing the equivalent control for the SMC schemes for SbW systems, which results in the control difficulty of the SbW control system for practical applications.

Inspired by above researches, in order to further improve the stability control performance of SbW vehicles via AFS system against parametric uncertainties and external disturbances, this paper focuses on the AFS-based ESC for SbW vehicles. The proposed vehicle stability control scheme consists of two parts: the upper controller and the lower controller. The upper controller (yaw stability control) adopts adaptive recursive integral terminal sliding mode (ARITSM) control with a sliding mode observer (SMO) for estimating the vehicle sideslip angle. It considers two controlled variables (vehicle sideslip angle and yaw rate) and only one control input (front steering angle), such that the sideslip angle and yaw rate can be driven to ideal values. In order to track the desired front wheel steering angle obtained from the upper controller, a novel fast nonsingular terminal sliding mode (FNTSM) control whose equivalent control is estimated via extreme learning machine (ELM) is developed as the lower controller for SbW systems. Although the ELM developed in this paper has a pretty similar structure to the classical one for pattern classifications whose input weights and hidden layer biases are randomly assigned [26]–[28], the output weights of the ELM will be online adjusted via designed adaptive laws in the sense of Lyapunov from the closed-loop system global stability point of view.

The main contributions of this paper are given as follows: (i) The proposed ARITSM-based upper controller of the ESC system not only guarantees the faster convergence rate and slighter control chattering than other SMC schemes, but also simultaneously considers the vehicle sideslip angle and yaw rate as control variables, such that better vehicle yaw stability and maneuverability can be achieved. (ii) By applying the lower FNTSM controller, both the strong robustness and excellent steering tracking of the SbW system can be well guaranteed. (iii) Due to the utilization of the ELM estimator to well estimate the equivalent control component of the FNTSM feedback control law, the design complexity of the lower controller is greatly simplified and the dependence of the SbW system dynamics on the lower controller design can be further alleviated, which is rather preferable for practical SbW applications.

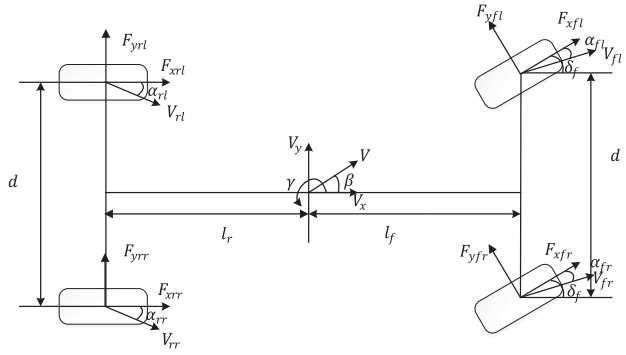

Fig. 1. 7DOF vehicle dynamic model.

The rest of this paper is organized as follows: In Section II, the vehicle dynamic model as well as SbW dynamic model are introduced. In Section III, the SMC-based AFS control strategy is proposed for the ESC of the SbW vehicles, where the upper and lower controllers are designed with the detailed stability proof presented based on Lyapunov theory. In Section IV, simulation results are carried out via Carsim and Matlab to verify the excellent performance of the proposed AFS-based ESC system, in comparison with several existing control strategies. Finally, Section V draws the conclusion.

II. Dynamical Modelling

In this section, both the vehicle dynamic model and the dynamic equation of SbW system are introduced in detail.

A. Vehicle Dynamic Model

In this part, a seven degree of freedom (7DOF) vehicle dynamic model is presented at first. Then the two degree of freedom (2DOF) vehicle dynamic model, called bicycle model, is implemented to simplify the dynamic model of 7DOF vehicle.

The 7 DOF dynamic model is proposed in Fig. 1. This model includes the motion equations of the longitudinal, lateral, yaw and four wheels of vehicle [29].

The longitudinal motion equation is modelled as:

$$m\,a_x = (F_{xfl} + F_{xfr})\cos\delta_f - (F_{yfl} + F_{yfr})\sin\delta_f + F_{xrl} + F_{xrr} + F_1 \tag{1}$$

The lateral motion is presented as:

$$m\,a_y = (F_{yfl} + F_{yfr})\cos\delta_f + (F_{xfl} + F_{xfr})\sin\delta_f + F_{yrl}$$

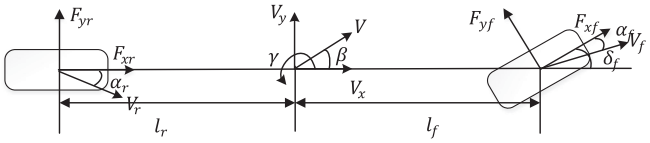

Fig. 2. 2DOF vehicle dynamic model.

$$+ F_{yrr} + F_2 \tag{2}$$

Then the yaw motion can be expressed as:

$$\begin{aligned} I_z \dot{\gamma} = & \left[\left(F_{xfl} + F_{xfr} \right) \sin \delta_f + \left(F_{yfl} + F_{yfr} \right) \cos \delta_f \right] l_f \\ & + \left[\left(F_{xfr} - F_{xfl} \right) \cos \delta_f + \left(F_{yfl} - F_{yfr} \right) \sin \delta_f \right] \frac{d}{2} \\ & + \left(F_{xrr} - F_{xfr} \right) \frac{d}{2} - \left(F_{yrl} + F_{yrr} \right) l_r + w \end{aligned} \tag{3}$$

where m is the total mass of vehicle, I_z is the moment of inertia around center of gravity (CG), V_x and V_y are the longitudinal and lateral velocities of the vehicle CG, V is the speed of vehicle. F_{xij} and F_{yij} are regarded as the longitudinal and lateral tire force, i represents front and rear, j represents left and right. d, l_f and l_r denote the track width, distance from the front and rear wheel axis to CG. Additionally, $\gamma, \delta_f, a_x, a_y$ are the yaw rate, front wheel steering angle, longitudinal and lateral acceleration respectively. F_1, F_2, and w are the bounded lumped disturbance including system uncertainties and external disturbance. Please note that this paper is devoted for the yaw stability control of the SbW vehicles and thus the lateral motion and the yaw motion should be focused on.

In general, assuming that the steering angle of front wheel is small enough, i.e., $\sin \delta_f \approx 0$, $\cos \delta_f \approx 1$, we express the vehicle sideslip angle β which is the angle between the traveling direction and longitudinal direction, as $\beta = \arctan(\frac{V_y}{V_x})$ [29]. Generally, $V_x \approx V \gg V_y$, thus $|\beta| \ll 1, \cos \beta \approx 1, \sin \beta \approx 0$. Therefore, the 7DOF vehicle dynamic model can be simplified as the 2DOF vehicle dynamic model in Fig. 2, which is convenient for the subsequent controller and observer designs.

Then, for 2DOF model of vehicle dynamics, F_{yfl} and F_{yrl} are obtained as [17]:

$$\begin{aligned} F_{yfl} &= C_f \alpha_{fl} = F_{yfr} = C_f \alpha_{fr} = F_{yf} = C_f \alpha_f \\ &= C_f \left(-\beta - \frac{l_f \gamma}{V_x} + \delta_f \right) \end{aligned} \tag{4}$$

$$\begin{aligned} F_{yrl} &= C_f \alpha_{rl} = F_{yrr} = C_f \alpha_{rr} = F_{yr} = C_r \alpha_r \\ &= C_r \left(-\beta + \frac{l_r \gamma}{V_x} \right) \end{aligned} \tag{5}$$

where C_f and C_r are the front and rear tire cornering stiffness. α_{ij} is the sideslip angle of front and rear tire. Assuming the vehicle speed V is a constant, the lateral acceleration a_y can be given by

$$a_y = V_x \gamma \cos \beta + \dot{V}_x \sin \beta + V_x \dot{\beta} \cos \beta \approx V_x \left(\gamma + \dot{\beta} \right) \tag{6}$$

Then substituting the equation (4)–(6) into(2) and (3), the lateral motion and yaw motion can be further expressed as:

$$\begin{aligned} m V_x \left(\gamma + \dot{\beta} \right) = & 2 \left[C_f \left(-\beta - \frac{l_f \gamma}{V_x} + \delta_f \right) \right] \\ & + 2 \left[C_r \left(-\beta + \frac{l_r \gamma}{V_x} \right) \right] + F_2 \end{aligned} \tag{7}$$

$$\begin{aligned} I_z \dot{\gamma} = & 2 C_f l_f \left(-\beta - \frac{l_f \gamma}{V_x} + \delta_f \right) \\ & - 2 C_r l_r \left(-\beta + \frac{l_r \gamma}{V_x} \right) + w \end{aligned} \tag{8}$$

For the ease of observer and controller design, the equations (7), (8) are rewritten as:

$$\begin{aligned} \dot{\beta} = & -\frac{2 \left(C_f + C_r \right)}{m V_x} \beta + \left[\frac{2 \left(C_r l_r - C_f l_f \right)}{m V_x^2} - 1 \right] \gamma \\ & + \frac{2 C_f}{m V_x} \delta_f + \frac{F_2}{m V_x} \end{aligned} \tag{9}$$

$$\begin{aligned} \dot{\gamma} = & \frac{2 \left(C_r l_r - C_f l_f \right)}{I_z} \beta + \frac{-2 \left(l_f^2 C_f + l_r^2 C_r \right)}{I_z V_x} \gamma \\ & + \frac{2 l_f C_f}{I_z} \delta_f + \frac{w}{I_z} \end{aligned} \tag{10}$$

Additionally, substituting the equation(9) into (6) yields:

$$a_y = -\frac{2 \left(C_f + C_r \right)}{m} \beta + \left[\frac{2 \left(C_r l_r - C_f l_f \right)}{m V_x} \right] \gamma + \frac{2 C_f}{m} \delta_f + \frac{F_2}{m} \tag{11}$$

Introducing the variables $X = [x_1 x_2]^T = [\beta \gamma]^T$, $Y = [y_1 \; y_2]^T = [\gamma \; a_y]$, $u = \delta_f$, the equations (9)-(11) can be rewritten in a state-space form as:

$$\begin{cases} \dot{X} = AX + Bu + D_1 \\ Y = CX + Eu + D_2 \end{cases} \tag{12}$$

where

$$A = \begin{bmatrix} -\frac{2(C_f + C_r)}{m V_x} & \frac{2(C_r l_r - C_f l_f)}{m V_x^2} - 1 \\ \frac{2(C_r l_r - C_f l_f)}{I_z} & \frac{-2\left(l_f^2 C_f + l_r^2 C_r \right)}{I_z V_x} \end{bmatrix} = \begin{bmatrix} a_{11} & a_{12} \\ a_{21} & a_{22} \end{bmatrix} \tag{13}$$

$$B = \begin{bmatrix} \frac{2 C_f}{m V_x} \\ \frac{2 l_f C_f}{I_z} \end{bmatrix} = \begin{bmatrix} b_1 \\ b_2 \end{bmatrix} \tag{14}$$

$$C = \begin{bmatrix} 0 & 1 \\ V_x a_{11} & V_x \left(a_{12} + 1 \right) \end{bmatrix} = \begin{bmatrix} c_{11} & c_{12} \\ c_{21} & c_{22} \end{bmatrix} \tag{15}$$

$$E = \begin{bmatrix} 0 \\ V_x b_1 \end{bmatrix} = \begin{bmatrix} E_1 \\ E_2 \end{bmatrix} \tag{16}$$

$$D_1 = \begin{bmatrix} \frac{F_2}{m V_x} \\ \frac{w}{I_z} \end{bmatrix} = \begin{bmatrix} d_1 \\ d_2 \end{bmatrix} \tag{17}$$

$$D_2 = \begin{bmatrix} 0 \\ \frac{F_2}{m} \end{bmatrix} = \begin{bmatrix} d_3 \\ d_4 \end{bmatrix} \tag{18}$$

The corresponding parameters of vehicle dynamics with their descriptions are shown in Table I.

TABLE I
PARAMETERS OF VEHICLE DYNAMICS

Symbol	Description
m	vehicle mass
I_z	moment of inertia around centre of gravity (CG)
V_x, V_y	longitudinal and lateral velocities of the vehicle CG
V	vehicle velocity
F_{xij},F_{yij}	longitudinal and lateral tire force
d	track width
l_f, l_r	distance from the front and rear wheel axis to CG
γ	yaw rate
δ_f	front wheel steering angle
a_y,a_x	lateral and longitudinal acceleration
$F_1, F_2 w$	bounded lumped disturbance including system uncertainties and external disturbance
β	Vehicle sideslip angle
$C_f \ \ C_r$	front and rear tire cornering stiffness
α_{ij}	front and rear tire sideslip angle
α_f, α_r	sideslip angle of front and rear tire

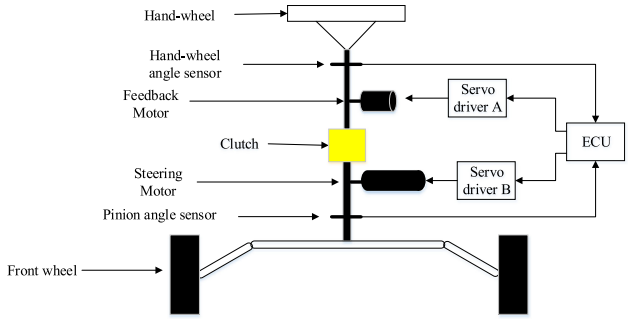

Fig. 3. SbW system model.

B. SbW System Dynamics

For a vehicle equipped with an SbW system, the front wheel steering angle δ_f consisting of the driver's steering angle command δ_{fd} and the corrected steering angle $\Delta\delta_{fd}$, is actually the control input of the AFS and the reference signal of the SbW system expressed as [3]:

$$\delta_f = \delta_{fd} + \Delta\delta_{fd} \tag{19}$$

Fig. 3 shows the SbW schematic model with a mechanical backup, where the clutch is designed to switch the steering system to the mechanical one for safety purpose when the SbW system malfunctions. A complete dynamic model of SbW system is detailedly reported in [22], which is given by

$$J_{eq}\ddot{\delta}_{ft} + B_{eq}\dot{\delta}_{ft} + \tau_e + \ \tau_f = k_c\tau \tag{20}$$

where τ_e and τ_f are the disturbances of SbW system. τ_e is the self-aligning moment generated by the tire cornering forces during turning, τ_f is the coulomb friction in the motor assembly and the steering system [24]. δ_{ft} is the actual front wheel steering angle, and τ is the motor control torque, while k_c is the combined ratio of the motor gearbox, rack and pinion gearbox. J_{eq} and B_{eq} are the total effective inertia and damping of the SBW system which are defined as:

$$J_{eq} = J_{fw} + k_c^2 J_{sm} \tag{21}$$

$$B_{eq} = B_{fw} + k_c^2 B_{sm} \tag{22}$$

where J_{fw} and J_{sm} are the moments of inertia of the front wheels and the steering motor, while B_{fw} and B_{sm} are the damping of the front wheels and the steering motor, respectively.

The parameters of SbW system with their descriptions are shown in Table II.

TABLE II
PARAMETERS OF SBW SYSTEM

Symbol	Description
δ_{ft}	actual front wheel steering angle
k_c	integrated ratio
τ	motor control torque
τ_f	coulomb friction torque
τ_e	self-aligning moment
J_{eq}	total effective inertia
B_{eq}	total effective damping
J_{fw}	moments of inertia of the front wheels
J_{sm}	moments of inertia of the steering motor
B_{fw}	damping of the front wheels
B_{sm}	damping of the steering motor

C. Control Objective

The control objective in this paper is to improve the yaw stability performance of SbW vehicles, such that both yaw rate and sideslip angle can approach the desired ones with a strong robustness again parameter uncertainties and disturbances.

Considering the tire/road condition, the desired yaw rate γ_d is given by [30]:

$$\gamma_d = \begin{cases} \gamma_t & \text{if } |\gamma_t| < \frac{0.85\mu g}{V_x} \\ \frac{\mu g}{V_x} sign\left(\gamma_t\right) & \text{if } |\gamma_t| \geq \frac{0.85\mu g}{V_x} \end{cases} \tag{23}$$

where μ is the tire-road friction coefficient and the γ_t is expressed as:

$$\gamma_t = \frac{V_x}{\left(1 + KV_x^2\right)\left(l_f + l_r\right)}\,\delta_{fd} \tag{24}$$

where δ_{fd} is the driver's steering angle command, $K = \frac{m(C_r l_r - C_f l_f)}{2(l_f + l_r)^2 C_f C_r}$ is the vehicle insufficient steering coefficient.

In this paper, the desired sideslip angle β_d is set as smaller as possible, which can be selected as zero to improve the lateral stability, i.e., $\beta_d = 0$.

As shown in (12), in order to achieve an excellent tracking performance, the front wheel steering angle δ_f is considered as the control signal, which is also the reference signal of the

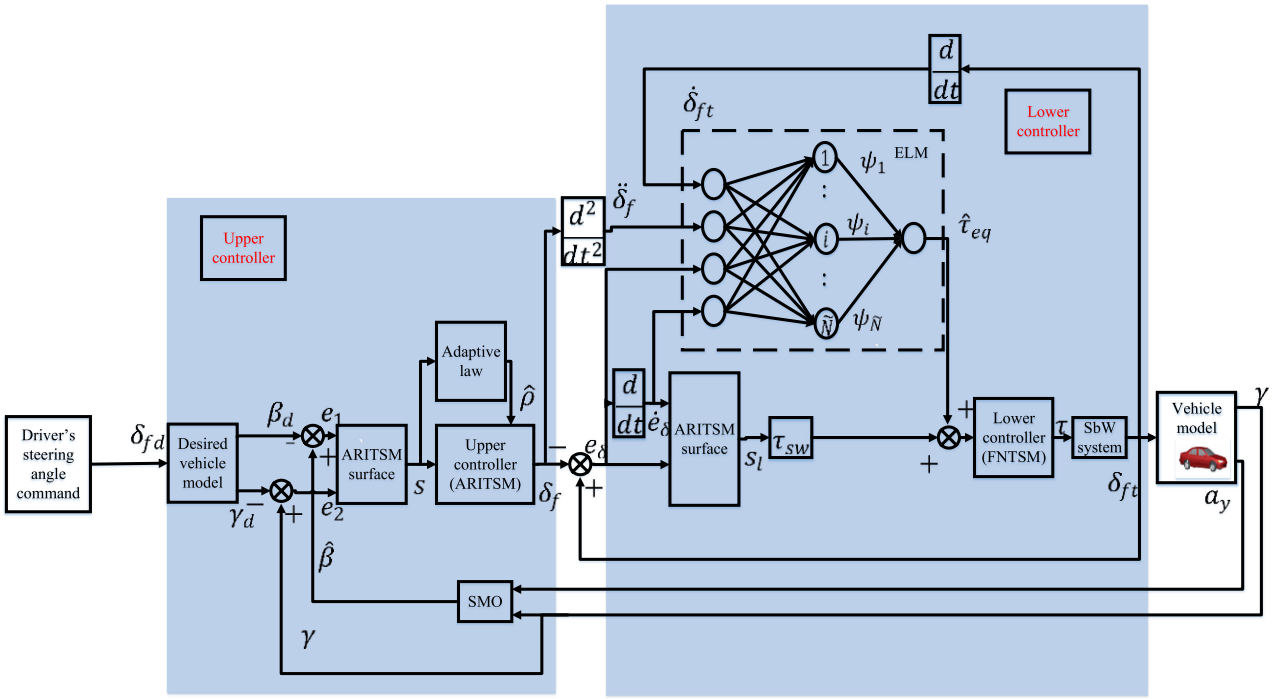

Fig. 4. Block diagram of the proposed ESC system.

SbW system. Thus, we also need to design a lower controller to guarantee that the actual front wheel steering angle δ_{ft} can track the reference with faster convergence rate and strong robustness such that the yaw stability of SbW vehicles can be achieved.

III. Control Scheme Design

A. SMO for Sideslip Angle Estimation

Since the sideslip angle β is hard to measure in practice, it is necessary to design an observer to identify and estimate its information. In this paper, we adopt the SMO developed in [31] to estimate the sideslip angle β.

$$\begin{cases} \dot{\hat{\beta}} = a_{11}\,\hat{\beta} + a_{12}\hat{\gamma} + b_1 u + k_1 k_2 sign\,(\tilde{\gamma}) + k_3\tilde{a}_y \\ \dot{\hat{\gamma}} = a_{21}\,\hat{\beta} + a_{22}\hat{\gamma} + b_2 u + k_1 sign\,(\tilde{\gamma}) + k_4\tilde{a}_y \\ \hat{a}_y = c_{21}\,\hat{\beta} + c_{22}\hat{\gamma} + E_2 u \end{cases} \tag{25}$$

where $\hat{\beta}$, $\hat{\gamma}$ and $\hat{a}_y$ are the estimated variables of β, γ and a_y respectively, k_i $(i = 1, 2, 3, 4) > 0$ are observer gains. Defining $\tilde{\beta} = \beta - \hat{\beta}, \tilde{\gamma} = \gamma - \hat{\gamma}$, and $\tilde{a}_y = a_y - \hat{a}_y$, the stability proof of the SMO can be easily obtained. Please refer to [31] for details.

Remark 1: Although the uncertainties, including external disturbances, modeling errors and sensor measuring errors, might affect the observer convergence characteristics leading to inaccurate estimation, the induced estimation errors will be inhibited by properly selecting k_i to satisfy the stability condition. In addition, the designed ARITSM control approach for the upper controller in the next section can also contribute to the alleviation of the effect of estimation errors for practical applications.

B. Upper Controller

The yaw stability control for SbW vehicles using ARITSM technique, as the upper controller, is designed to guarantee the vehicle stability, which considers two controlled variables (sideslip angle and yaw rate) and only one control input (front steering angle). In other words, the upper control object is to obtain fast and accurate tracking performance of the vehicle sideslip angle and yaw rate.

Firstly, we define the tracking errors between the actual sideslip angle β, yaw rate γ and their reference values as:

$$e_1 = \hat{\beta} - \beta_d = \hat{\beta} \tag{26}$$

$$e_2 = \gamma - \gamma_d \tag{27}$$

Combining (26), (27) with (12), the error dynamics can be given by:

$$\dot{e}_1 = \dot{\hat{\beta}} = \dot{\beta} - \dot{\tilde{\beta}} = a_{11}\,\beta + a_{12}\gamma + b_1\delta_f + d_1 - \dot{\tilde{\beta}} \tag{28}$$

$$\dot{e}_2 = \dot{\gamma} - \dot{\gamma}_d = a_{21}\,\beta + a_{22}\gamma + b_2\delta_f + d_2 - \dot{\gamma}_d \tag{29}$$

To construct the ARITSM controller, we first introduce the following sliding function σ,which consider two controlled variables, given by:

$$\sigma = ae_1 + e_2 \tag{30}$$

where $a > 0$ is the weight coefficient reflecting the proportion of sideslip angle deviation.

Then, a recursive integral terminal sliding function s is defined as follows [32]:

$$s = \sigma + \lambda\sigma_I \tag{31}$$

σ_I is given as:

$$\dot{\sigma}_I = sig(\sigma)^b = |\sigma|^b sign\,(\sigma) \tag{32}$$

where the parameters $\lambda > 0$, $0 < b < 1$.

Note that if we choose the initial value of integral element $\dot{\sigma}_I$ as follows, the reaching time will be eliminated.

$$\sigma_I\ (0) = -\lambda^{-1}\sigma\ (0) = ae_1\,(0) + e_2\,(0) \tag{33}$$

The derivative of the recursive integral terminal sliding function s is expressed as:

$$\begin{aligned}\dot{s} = \dot{\sigma} + \lambda\,\dot{\sigma}_I &= a\left(a_{11}\beta + a_{12}\gamma + b_1\delta_f + d_1 - \dot{\tilde{\beta}}\right) + a_{21}\beta \\ &+ a_{22}\gamma + b_2\delta_f + d_2 - \dot{\gamma}_d + \lambda|\sigma|^b sign\,(\sigma) \\ &= (a_{21} + aa_{11})\left(\hat{\beta} + \tilde{\beta}\right) + (a_{22} + aa_{12})\,\gamma - \dot{\gamma}_d + \lambda|\sigma|^b \\ &\times sign\,(\sigma) + ad_1 + d_2 - a\dot{\tilde{\beta}} + (b_2 + ab_1)\,\delta_f \end{aligned} \tag{34}$$

Substituting (33) into (31), it can be obtained that the sliding variable $s(0) = 0$. This implies that the control system is enforced to start on the sliding surface at the initial time such that the reaching time is eliminated [33].

Finally, the controller is design as

$$u = \delta_f = \frac{1}{b_2 + ab_1}\Bigg[-(a_{21} + aa_{11})\,\hat{\beta} - (a_{22} + a_{12}a)\,\gamma + \dot{\gamma}_d - \lambda|\sigma|^b sign\,(\sigma) - \hat{\rho} sign\,(s)\Bigg] \tag{35}$$

where $\hat{\beta}$ is the estimated vehicle sideslip angle from SMO and $\hat{\rho}$ is the estimation of the desired switching gain ρ to be updated by the following adaptive law:

$$\dot{\hat{\rho}} = \eta_1\,|s| \tag{36}$$

where η_1 is the positive constant defined as adaption rate.

Lemma 1: An upper bound always exists for $\hat{\rho}$, i.e., there exists a positive number ρ such that $\hat{\rho} \le \rho$ always holds. Proof of Lemma 1 is shown as follows [32]:

Proof of Lemma 1: Assuming $|s| \neq 0$, we can see from equation (36)that $\hat{\rho}$ is increasing and there must exist a time t_0 such that:

$$\hat{\rho}\,(t_0) > |D| \tag{37}$$

If $t = t_0,$ the adaptation gain $\hat{\rho}$ will be large enough to make the $|s|$ decreasing based on the derivative s in (34). Then $\hat{\rho}$ will continue to increase until $s = 0$ in a finite time Δt. Finally, the $\hat{\rho}$ stops increasing in the final value $\hat{\rho}(t_0 + \Delta t)$. That means the $\hat{\rho}$ has an upper bound, i.e., $\hat{\rho} \le \hat{\rho}(t_0 + \Delta t)$, thus we can choose the upper bound as ρ, i.e., $\hat{\rho} \le \rho = \bar{D}$.

The Proof of Lemma 1 is completed.

Theorem 1: If the sliding mode surface is designed as (31) and the closed-loop control law for the upper ESC scheme is proposed as (35), both two sliding functions s and σ will converge to zero in a finite time.

Proof: Substituting (35) into (34), it yields:

$$\begin{aligned}\dot{s} &= (a_{21} + aa_{11})\,\tilde{\beta} - a\dot{\tilde{\beta}} + ad_1 + d_2 - \hat{\rho} sign\,(s) \\ &= D - \hat{\rho} sign\,(s)\end{aligned} \tag{38}$$

where D denotes all system internal and external uncertainties, which is expressed as:

$$D = (a_{21} + aa_{11})\,\tilde{\beta} - a\dot{\tilde{\beta}} + ad_1 + d_2 \tag{39}$$

And the desired switching gain ρ is shown as:

$$\rho = \bar{D}\ > |D| \tag{40}$$

$\bar{D}$ is an unknown but bounded positive number.

Proof of controller stability: define the adaptive estimation error $\tilde{\rho} = \rho - \hat{\rho} = \bar{D} - \hat{\rho} \ge 0$ and choose the Lyapunov function $V = \frac{1}{2}\,s^2 + \frac{1}{2}\mu\tilde{\rho}^2$, where μ is a positive number.

The time derivative of V is given as:

$$\dot{V} = s\dot{s} + \mu\tilde{\rho}\dot{\tilde{\rho}} \tag{41}$$

Substituting (38) and considering $\dot{\tilde{\rho}} = -\dot{\hat{\rho}}$

$$\begin{aligned}\dot{V} &= s\,[D - \hat{\rho} sign\,(s)] - \mu\tilde{\rho}\dot{\hat{\rho}} \le |D|\,|s| - \hat{\rho}\,|s| - \bar{D}\,|s| \\ &+ \bar{D}\,|s| - \mu\tilde{\rho}\dot{\hat{\rho}} \\ &= |D|\,|s| + \tilde{\rho}\,|s| - \bar{D}\,|s| - \eta_1\mu\tilde{\rho}\,|s| \\ &= -\left(\bar{D} - |D|\right)|s| - (\eta_1\mu - 1)\,|s|\,\tilde{\rho} \\ &= -\sqrt{2}\left(\bar{D} - |D|\right)\frac{|s|}{\sqrt{2}} - \sqrt{\frac{2}{\mu}}\,(\eta_1\mu - 1)\,|s|\sqrt{\frac{\mu}{2}}\tilde{\rho} \\ &\le -\Gamma\left(\frac{|s|}{\sqrt{2}} + \sqrt{\frac{\mu}{2}}\tilde{\rho}\right) \le -\Gamma\sqrt{V}\end{aligned} \tag{42}$$

where $\eta_1\mu > 1$ and $\Gamma = \min\{\sqrt{2}(\bar{D} - |D|),\ \sqrt{\frac{2}{\mu}}(\eta_1\mu - 1)|s|\} > 0$.

The inequality (42) satisfies the finite time stability criterion [34]. Consequently, V reaches zero in a finite time t_r that is bounded by:

$$t_r \le \frac{2\sqrt{V\,(0)}}{\Gamma} \tag{43}$$

Furthermore, the sliding variable s will converge to zero in a finite time, after that it can be verified that σ can converge to zero as well.

The proof is completed.

Remark 2: Although the variable s and σ will converge to zero in a finite time, it does not theoretically imply that the sideslip angle β and yaw rate γ converge to their reference ones in a finite time. However, by properly tuning the parameter a in (30), we can ensure the two controlled variables to approach as much as possible to their desired values in the sliding mode. The following two facts have been noted: (i) It will be seen from the simulation results that β and γ are quite closed to their desired values after s and σ converge to zero. (ii) As has been shown in previous researches [35], [36] and revealed in this study, by combining the sideslip angle and yaw rate as the control objective, better stability performance can be obtained

when compared with the case of using only one of these values alone.

Remark 3: Compared to the traditional SMC schemes [31], [35], [36] whose control objects are also β and γ, the proposed ARITSM control can not only guarantee the stronger robustness, but also reduce the reaching time by designing the ARITSM surface to eliminate the reaching phase. Also, since the integral element in (32) is a continuous function, the chattering phenomenon can also be decreased further. In addition, by using the adaptive law (36), the bound of uncertainty information can be estimated successfully in the sense of Lyapunov, which can overcome the difficulty of choosing the desired switching gain for practical applications.

C. Lower Controller

According to the above description, the designed control input of the upper controller δ_f can enable the actual sideslip angle β and yaw rate γ to track the desired ones, such that the vehicle stability and maneuverability can be well guaranteed. In order to obtain the ideal δ_f for SbW vehicles, a robust controller should be required to guarantee the actual front wheel steering angle of the SbW system to closely converge to the ideal one, which is actually the control target of the lower controller.

In this paper, a novel FNTSM control methodology whose equivalent control is estimated via ELM is proposed as the lower controller for SbW vehicle to achieve the excellent tracking of the front wheel steering angle.

1) Basic Theory of ELM: Before proceeding the controller design, we first introduce the basic theory of extreme learning machine.

For N arbitrary distinct samples $(\boldsymbol{z}_j, \boldsymbol{t}_j)$, if an SLFN with $\tilde{N}$ hidden nodes can approximate these Nsamples with no error, it can be expressed as:

$$\sum_{i=1}^{\tilde{N}} \psi_i G\ (\boldsymbol{w}_i \boldsymbol{z}_j + c_i) = \boldsymbol{t}_j,\ j = 1, \ldots, N. \tag{44}$$

where $\boldsymbol{z}_i = [z_{i1}, z_{i2}, \ldots, z_{in}]^T \in R^n$ is the input and $\boldsymbol{t}_i = [t_{i1}, t_{i2}, \ldots, t_{im}]^T \in R^m$ is the output, $\boldsymbol{w}_i = [w_{i1}, w_{i2}, \ldots, w_{in}]^T$ is the input weight vector, c_i are input bias of the hidden nodes, $\psi_i = [\psi_{i1}, \psi_{i2}, \ldots, \psi_{im}]^T$ is the output weight vector connecting the ith hidden node and the output nodes, and $G(\cdot)$ is the activation function[26].

The equation (44) can be rewritten compactly as:

$$\boldsymbol{H}\boldsymbol{\psi} = \boldsymbol{T} \tag{45}$$

where $\mathbf{H}$ is called the hidden layer output matrix of the neural network, $\boldsymbol{\psi} = [\psi_1^T, \ldots, \psi_{\tilde{N}}^T]^T \in R^{\tilde{N}\times m}$, and $\mathbf{T} = [\boldsymbol{t}_1^T, \ldots, \boldsymbol{t}_N^T]^T \in R^{N\times m}$.

$$\boldsymbol{H} = \begin{bmatrix} G(\boldsymbol{z}_1, \boldsymbol{w}_1, c_1) & \cdots & G(\boldsymbol{z}_1, \boldsymbol{w}_{\tilde{N}}, c_{\tilde{N}}) \\ \vdots & \cdots & \vdots \\ G(\boldsymbol{z}_N, \boldsymbol{w}_1, c_1) & \cdots & G(\boldsymbol{z}_N, \boldsymbol{w}_{\tilde{N}}, c_{\tilde{N}}) \end{bmatrix} \in R^{N\times\tilde{N}} \tag{46}$$

The ELM algorithm has the following property [26]: Given any small positive value ϵ, and infinitely differentiable activation function $G(\cdot)$, there exists $\tilde{N} \le N$ such that for N arbitrary distinct samples $(\boldsymbol{z}_i, \boldsymbol{t}_i)$, for any $\boldsymbol{w}$ and $\boldsymbol{c}$ chosen from any intervals of $\boldsymbol{R}^{\mathrm{n}}$ and $\boldsymbol{R}$, respectively, according to any continuous probability distribution, then with probability one:

$$\|\boldsymbol{H}(\boldsymbol{z}, \boldsymbol{w}, \boldsymbol{c})\boldsymbol{\psi} - \boldsymbol{T}\| = \|\epsilon(\boldsymbol{z})\| < \epsilon \tag{47}$$

2) FNTSM Controller Design: Firstly, we define the tracking error between the actual front wheel steering angle δ_{ft} and its reference δ_f as

$$\begin{cases} e_\delta = \delta_{ft} - \delta_f \\ \dot{e}_\delta = \dot{\delta}_{ft} - \dot{\delta}_f \end{cases} \tag{48}$$

Given the system model in (20), we obtain the error dynamics of the closed-loop SbW system as follows:

$$\ddot{e}_\delta = \frac{1}{J_{eq}}\left(-B_{eq}\dot{\delta}_{ft} - \tau_e - \tau_f + k_c\tau\right) - \ddot{\delta}_f \tag{49}$$

Then the FNTSM surface is designed as [37]:

$$s_l = e_\delta + l_1|\dot{e}_\delta|^{\lambda_1} sign(\dot{e}_\delta) + l_2|e_\delta|^{\lambda_2} sign(e_\delta) \tag{50}$$

where $l_1 > 0$, $l_2 > 0$, $1 < \lambda_1 < 2$, $\lambda_2 > \lambda_1$, and λ_1 is chosen as $\lambda_1 = q/p$ with q and p being positive odd numbers.

If all the parameters and uncertainties of the SbW system dynamic model in (20) can be obtained precisely, the controller can be designed as follows:

$$\tau = \tau_{eq}^* + \tau_{sw} \tag{51}$$

where

$$\tau_{eq}^* = \frac{B_{eq}}{k_c}\dot{\delta}_{ft} + \frac{\tau_e + \tau_f}{k_c} + \frac{J_{eq}}{k_c}\ddot{\delta}_f - \frac{J_{eq}}{k_c l_1 \lambda_1}|\dot{e}_\delta|^{1-\lambda_1} (1 + l_2\lambda_2|e_\delta|^{\lambda_2 - 1})\dot{e}_\delta \tag{52}$$

$$\tau_{sw} = -\varphi sign(s_l) \tag{53}$$

where τ_{eq}^* and τ_{sw} are the equivalent and compensation control of the FNTSMC, φ is a positive constant.

However, it is always unavailable to obtain all the accurate parameters and uncertainties in a real SbW system. It means that the equivalent control in (52) cannot be well implemented for practical situation. To solve this problem, this paper proposes an ELM based-estimator to approximate the ideal equivalent control in the closed-loop control of the lower controller.

The estimation of the equivalent control $\hat{\tau}_{eq}$ is designed as:

$$\hat{\tau}_{eq} = \boldsymbol{H}(\boldsymbol{z}, \boldsymbol{w}, c)\hat{\boldsymbol{\psi}} \tag{54}$$

where $\hat{\boldsymbol{\psi}}$ is updated by the following adaptive law:

$$\dot{\hat{\boldsymbol{\psi}}}^T = -\eta_2 l_1 \lambda_1 |\dot{e}_\delta|^{\lambda_1 - 1} s\boldsymbol{H}(\boldsymbol{z}, \boldsymbol{w}, c) \tag{55}$$

where the learning rate $\eta_2 > 0$, and the input vector $\mathbf{z} = [e_\delta\ \dot{e}_\delta\ \dot{\delta}_{ft}\ \ddot{\delta}_f]^{\mathbf{T}}$.

Thus, the lower controller (51) becomes:

$$\tau = \hat{\tau}_{eq} + \tau_{sw} \tag{56}$$

According to the universal approximation theorem of SLFN in [26], there exists the optimal output weight parameters $\boldsymbol{\psi}^*$ to

estimate the equivalent control τ_{eq}^*.

$$\tau_{eq}^* = \boldsymbol{H}\left(\boldsymbol{z}, \boldsymbol{w}, c\right)\boldsymbol{\psi}^* + \epsilon\left(\boldsymbol{z}\right) \tag{57}$$

where the estimation error $||\epsilon(\mathbf{z})|| \leq \epsilon$.

Before stability analysis, the error of output weights is defined as $\tilde{\boldsymbol{\psi}} = \boldsymbol{\psi}^* - \hat{\boldsymbol{\psi}}$.

The derivative of s_l is expressed as:

$$\begin{aligned}\dot{s}_l &= \dot{e}_\delta + l_1\lambda_1|\dot{e}_\delta|^{\lambda_1-1}\ddot{e}_\delta + l_2\lambda_2|e_\delta|^{\lambda_2-1}\dot{e}_\delta \\ &= \dot{e}_\delta \ + l_2\lambda_2|e_\delta|^{\lambda_2-1}\dot{e}_\delta + l_1\lambda_1|\dot{e}_\delta|^{\lambda_1-1} \\ &\quad \times \left[\frac{1}{J_{eq}}\left(-B_{eq}\dot{\delta}_{ft} - \tau_e - \tau_f + k_c\tau\right) - \ddot{\delta}_f\right]\end{aligned} \tag{58}$$

Substituting (54), (56) and (57) into (58), it can be obtained that:

$$\begin{aligned}\dot{s}_l &= \dot{e}_\delta + l_2\lambda_2|e_\delta|^{\lambda_2-1}\dot{e}_\delta + l_1\lambda_1|\dot{e}_\delta|^{\lambda_1-1} \\ &\quad \times \left\{\frac{1}{J_{eq}}[-B_{eq}\dot{\delta}_{ft} - \tau_e - \tau_f \right. \\ &\quad \left. + \left(k_c\left(\boldsymbol{H}\hat{\boldsymbol{\psi}} - \varphi sign\left(s_l\right)\right)\right] - \ddot{\delta}_f\right\} \\ &= \dot{e}_\delta + l_2\lambda_2|e_\delta|^{\lambda_2-1}\dot{e}_\delta + l_1\lambda_1|\dot{e}_\delta|^{\lambda_1-1} \\ &\quad \times \left\{\frac{1}{J_{eq}}[-B_{eq}\dot{\delta}_{ft} - \tau_e - \tau_f + (k_c(\boldsymbol{H}\hat{\boldsymbol{\psi}} - \varphi sign\left(s_l\right) \right. \\ &\quad \left. + \boldsymbol{H}\boldsymbol{\psi}^* + \epsilon\left(\boldsymbol{z}\right) - \boldsymbol{H}\boldsymbol{\psi}^* - \epsilon\left(\boldsymbol{z}\right))] - \ddot{\delta}_f\right\} \\ &= \frac{l_1\lambda_1|\dot{e}_\delta|^{\lambda_1-1}k_c}{J_{eq}}\left[-\varphi sign\left(s_l\right) + \boldsymbol{H}\hat{\boldsymbol{\psi}} - \boldsymbol{H}\boldsymbol{\psi}^* - \epsilon\left(\boldsymbol{z}\right)\right] \\ &= \frac{l_1\lambda_1|\dot{e}_\delta|^{\lambda_1-1}k_c}{J_{eq}}\left[-\varphi sign\left(s_l\right) - \boldsymbol{H}\tilde{\boldsymbol{\psi}} - \epsilon\left(\boldsymbol{z}\right)\right]\end{aligned} \tag{59}$$

Theorem 2: If the sliding mode surface is chosen as in (50), and the lower controller is designed as in (56) and the output weight $\hat{\boldsymbol{\psi}}$ of the ELM is updated by the adaptive law in (55), then the closed-loop SbW error dynamics in (49) will reach the sliding mode surface in a finite time. Thereafter, the steering tracking error will converge to zero in a finite time along $s_l = 0$.

Proof: Choose the Lyapunov function $V_l = \frac{J_{eq}}{2k_c}\ s_l^2 + \frac{1}{2\eta_2}\tilde{\boldsymbol{\psi}}^T\tilde{\boldsymbol{\psi}}$, where η_2 is a positive number.

The time derivative of V_l is given as:

$$\dot{V}_l = \frac{J_{eq}}{k_c}\ s_l\dot{s}_l + \frac{1}{\eta_2}\dot{\tilde{\boldsymbol{\psi}}}^T\tilde{\boldsymbol{\psi}} \tag{60}$$

Substituting equation (55) and (59) and considering $\dot{\tilde{\boldsymbol{\psi}}}^T = -\dot{\hat{\boldsymbol{\psi}}}^{\mathrm{T}}$:

$$\begin{aligned}\dot{V}_l &= \frac{J_{eq}}{k_c}\ s_l\left[\frac{l_1\lambda_1|\dot{e}_\delta|^{\lambda_1-1}k_c}{J_{eq}}\left(-\varphi sign\left(s_l\right) - \boldsymbol{H}\tilde{\boldsymbol{\psi}} - \epsilon\left(\boldsymbol{z}\right)\right)\right] \\ &\quad + l_1\lambda_1|\dot{e}_\delta|^{\lambda_1-1}s_l\boldsymbol{H}\tilde{\boldsymbol{\psi}} = l_1\ \lambda_1|\dot{e}_\delta|^{\lambda_1-1}\left[-\varphi\left|s_l\right| - s_l\epsilon\left(\boldsymbol{z}\right)\right] \\ &\leq l_1\lambda_1|\dot{e}_\delta|^{\lambda_1-1}\left[-\varphi\left|s_l\right| + \left|\epsilon\left(\boldsymbol{z}\right)\right|\left|s_l\right|\right] \\ &\leq -\ l_1\lambda_1|\dot{e}_\delta|^{\lambda_1-1}\left|s_l\right|\left(\varphi - \epsilon\right)\langle -\sigma \text{ for } \left|s_l\right| \neq 0, |\ \dot{e}_\delta| \neq 0\end{aligned} \tag{61}$$

where $||\epsilon(\mathbf{z})|| \leq \epsilon$, and $l_1\lambda_1|\dot{e}_\delta|^{\lambda_1-1}|s_l|(\varphi - \epsilon) > \sigma, \sigma > 0$.

Then if $\dot{e}_\delta = 0$, the error dynamics (49) can be expressed as:

$$\begin{aligned}\ddot{e}_\delta &= \frac{1}{J_{eq}}\left[-B_{eq}\dot{\delta}_{ft} - \tau_e - \tau_f + (k_c(\boldsymbol{H}\hat{\boldsymbol{\psi}} - \varphi sign\left(s_l\right)\right. \\ &\quad \left. + \boldsymbol{H}\boldsymbol{\psi}^* \ + \epsilon\left(\boldsymbol{z}\right) - \boldsymbol{H}\boldsymbol{\psi}^* - \epsilon\left(\boldsymbol{z}\right))] - \ddot{\delta}_f \\ &= \frac{1}{J_{eq}}\left[k_c\left(-\varphi sign\left(s_l\right) - \boldsymbol{H}\tilde{\boldsymbol{\psi}} - \epsilon\left(\boldsymbol{z}\right)\right)\right] \neq 0\end{aligned} \tag{62}$$

which means that the $\dot{e}_\delta = 0$ is not an attractor in the reaching phase.

It is obvious that the controller (56) can drive the variable s_l to zero in a finite time and will keep it at zero thereafter. Then the tracking error between actual front wheel steering angle δ_{ft} and its reference δ_f will converge to zero alongside the FNTSM surface (50) with a faster convergence rate and strong robustness [38].

Here completes the proof.

Remark 4: Compared with the traditional linear SMC schemes which only guarantee the tracking error to asymptotically converge to zero [23], [24], the proposed FNTSM control can achieve faster convergence characteristics. Also, considering that the SbW system dynamics should be known precisely in the process of designing the equivalent control of the traditional sliding mode control, a novel estimator via the ELM is proposed in this paper to adaptively estimate the equivalent control such that the dependence of system dynamics can be nicely alleviated, which significantly facilitates the sliding mode control for practical applications.

Remark 5: It is noted that the implementation of the ELM is serving as the equivalent control estimator, whose output weight $\boldsymbol{\psi}$ is updated by the adaptive law (55) in Lyapunov sense from the perspective of global stability of the closed loop system, which is different from the conventional ELM whose $\boldsymbol{\psi}$ is offline updated by the least-square method with batch training data. However, the input weights and hidden layer biases of the proposed ELM can still be randomly assigned like the original ELM, which remains the advantages of ELM technique.

Remark 6: Both the upper controller in (35) and the lower controller in (56) contain the signum function, which can cause the control chattering. In this paper, the saturation function is used to replace the signum function to alleviate the chattering phenomenon, which is expressed as:

$$sat\ \left(s\right) = \begin{cases} \frac{s}{\xi} & \text{for } |s| < \xi \\ sign\left(s\right) & \text{for } |s| \geq \xi \end{cases} \tag{63}$$

where $\xi > 0$ is a boundary layer constant to be properly tuned, such that a tradeoff between the control smoothness and the tracking precision should be taken.

Remark 7: It is noted that the control parameters of both the upper controller in (35) and the lower controller in (56) should be selected properly to obtain the best stability control

performance. The corresponding parameter selection criteria are shown below in detail. 1) For the upper controller, the weight coefficient a reflects the proportion of the sideslip angle deviation. If the vehicle experiences a large tire-road friction coefficient μ, smaller value of a is required to decrease the effect of sideslip angle. 2) The larger value of λ and smaller value of b, the faster σ convergence rate, but overlarge values would bring large control amplitude. 3) The adaption rate η_1 should be normally chosen large enough to enhance the update rate of $\hat{\rho}$ have a fast update rate, but a reasonable range should be taken into consideration for maintaining the close-loop stability. 4) For the lower controller, φ should be chosen large enough to resist large uncertain disturbances, but too large value will cause the overlarge control amplitude. 5) For $\lambda_1,\ \lambda_2,\ l_1$ and l_2, larger values would enhance the convergence rate, but too large values may affect the closed-loop stability. 6) Large learning rate η_2 can guarantee fast learning speed but may cause overshoot or even instability of the closed-loop output weight $\hat{\psi}$, thus it should be selected properly to balance the relationship between the learning speed and closed-loop system stability. 7) Theoretically, the bigger $\tilde{N}$, the more excellent estimation accuracy, but overlarge value may increase computation burden which slows down the estimation speed in the real-time control system.

Remark 8: The superiorities of all the components in the control scheme are detailed described as follows: (i) Due to the introduction of an integral element in the proposed ARITSM, not only can the reaching time be reduced, but also the chattering phenomenon can be decreased further. (ii) The bound of uncertainty information in the upper controller can be estimated successfully in the sense of Lyapunov by using the adaptive law which relaxes prior knowledge of the system uncertainty required for conventional sliding mode controller design. (iii) As for the lower controller, the proposed FNTSM control achieves faster convergence characteristics compared with the traditional linear SMC schemes. Besides, a novel estimator via the ELM is proposed to adaptively estimate the equivalent control component such that the dependence of system dynamics can be nicely alleviated. All the above features of the proposed control reveal the better stability performance of the SbW vehicles, with respective to error convergence rate, robustness towards uncertainty and easy implementation compared with other control methods.

The block diagram of the proposed ESC system is detailed depicted in Fig. 4 and the corresponding stability control performance of SbW vehicles will be fully verified by simulation studies in the subsequent section.

IV. Simulation Results and Analyses

In order to verify the excellent performance of the proposed control scheme, a series of simulations are carried out by utilizing Carsim and Matlab software and the detailed result analyses are shown in this section. For evaluating the stability control performance, the traditional sliding mode control methods considering two controlled variables and only one control input variable, are also given for the upper controller of the yaw stability control scheme.

TABLE III
Key Parameters of Vehicle Model in Carsim

Parameter	Value
$m(kg)$	1274
$I_z(kg.m^2)$	1523
$V(km/h)$	54
$d(m)$	1.539
$l_f, l_r(m)$	1.016,1.562
$C_f(N/rad)$	57000
$C_r(N/rad)$	68000
μ	0.6

TABLE IV
Controller Parameters

Controller	Parameter	Value
ARITSMC	a	0.1
	b	0.5
	λ	0.5
	η_1	30
SMC1	a_1	0.1
	ρ_1	100
SMC2	ς	10
	ρ_2	20
Lower controller	l_1	0.1
	l_2	0.01
	λ_1	19/17
	λ_2	17/11
	φ	50
	η_2	40

The first traditional sliding mode controller (SMC1) considering two controller variables is designed as:

$$u_1 = \frac{1}{(a_1 b_1 + b_2)}\Big[-(a_1 a_{11} + a_{21})\,\hat{\beta} - (a_1 a_{12} + a_{22})\,\gamma + \dot{\gamma}_d - \rho_1 sign(s_1)\Big] \tag{64}$$

where $a_1 > 0$ is the weight coefficient, $\rho_1 > 0$ and the sliding mode surface s_1 is designed as:

$$s_1 = a_1\,\hat{\beta} + (\gamma - \gamma_d) \tag{65}$$

The second sliding mode controller (SMC2) which only considers the yaw rate is designed as:

$$u_2 = \frac{1}{b_2}\Big[a_{21}\hat{\beta} - a_{22}\gamma + \dot{\gamma}_d - \varsigma(\dot{\gamma} - \dot{\gamma}_d) - \rho_2 sign(s_2)\Big] \tag{66}$$

where the sliding mode surface s_2 is designed as:

$$s_2 = (\dot{\gamma} - \dot{\gamma}_d) + \varsigma(\gamma - \gamma_d) \tag{67}$$

where $\varsigma > 0$ and $\rho_2 > 0$.

The key parameters of the vehicle model in Carsim and all the controller parameters are listed in Table III and Table IV, respectively.

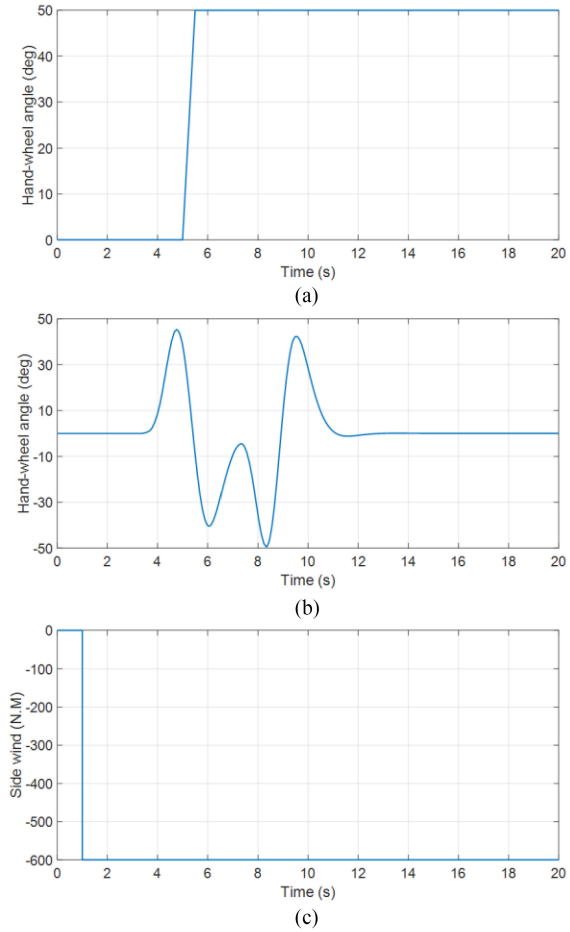

Fig. 5. Hand-wheel angle and disturbance input. (a) J-turn maneuver. (b) Double-lane change maneuver. (c) Sidewind disturbance.

According to the typical driving behaviors, two practical hand-wheel inputs are considered which are shown in Fig. 5 (a) and (b). The first maneuver is J-turn maneuver and the other is double-lane change maneuver. In order to test the control robustness, a side wind disturbance is considered in the J-turn and double-lane change maneuvers as shown in Fig. 5(c).

A. J-Turn Maneuver With/Without Side Wind Disturbance

Under J-turn maneuver without considering the effect of side wind disturbance, the simulation results are shown in Fig. 6 by applying the proposed controller (35), and the two comparative controllers (64) and (66).

It is obvious that the control performance of the proposed control strategy is superior to other two controllers, since not only is the actual yaw rate closest to its desired value, but also the smallest sideslip angle is achieved, as clearly shown in Fig. 6(a), (b) and (c). We can also observe that the proposed control obtains nearly zero tracking error of the yaw rate and the maximum yaw rate error (MYRE), i.e., max ($|e_2|$), is 0.131 deg/s, while the SMC2 exhibits the worst yaw tracking performance with the MYRE value of 1.52 deg/s. followed by the SMC1 with MYRE value of 0.517 deg/s. As shown in Fig. 6 (d), the proposed control obtains best trajectory tracking performance for J-turn maneuver

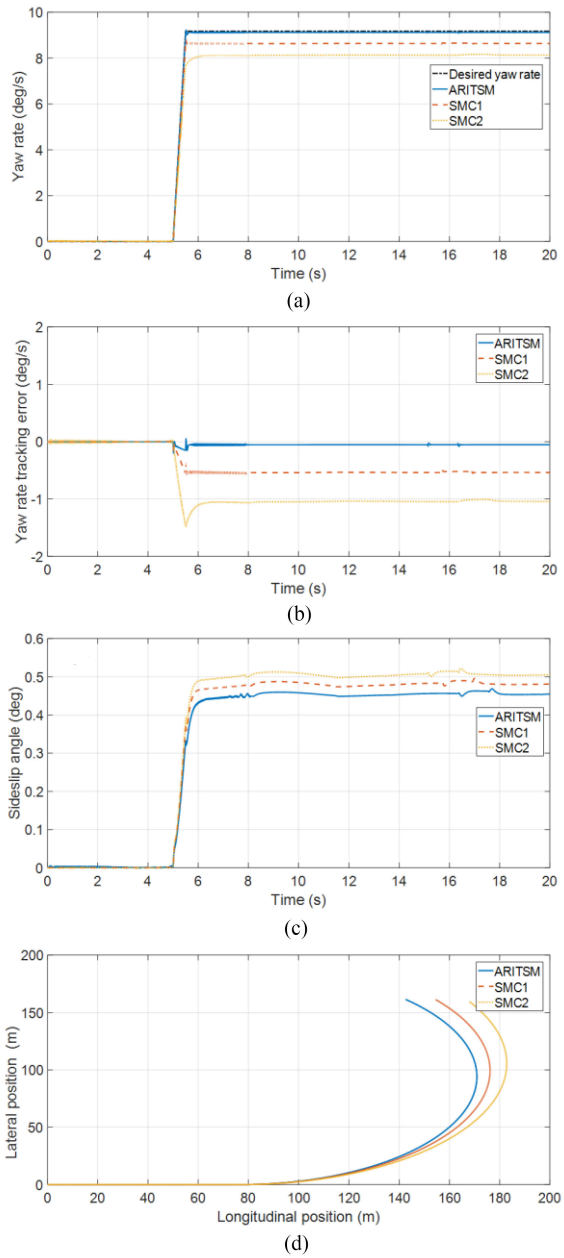

Fig. 6. Control performance of all controllers in J-turn maneuver without side wind disturbance. (a) The response curves of yaw rate. (b) The yaw rate tracking error. (c) The response curves of sideslip angle. (d) The vehicle trajectory.

while other two controllers perform a large trajectory deviation due to the large yaw rate error and sideslip angle. In addition, by comparing the simulation results of SMC1 and SMC2, it can also be found that a better performance can be obtained via combining sideslip angle and yaw rate as the control objective as compared with the case of using only one of these values.

Then, the side wind disturbance is added to compare the robustness of the proposed control with other two SMC methods. Fig. 7 shows the simulation results under different controllers with the side wind disturbance. It is shown that similar control performance is obtained for the proposed controller compared with that without disturbance shown in Fig. 6, but other two controllers have much worse performance especially SMC2. By

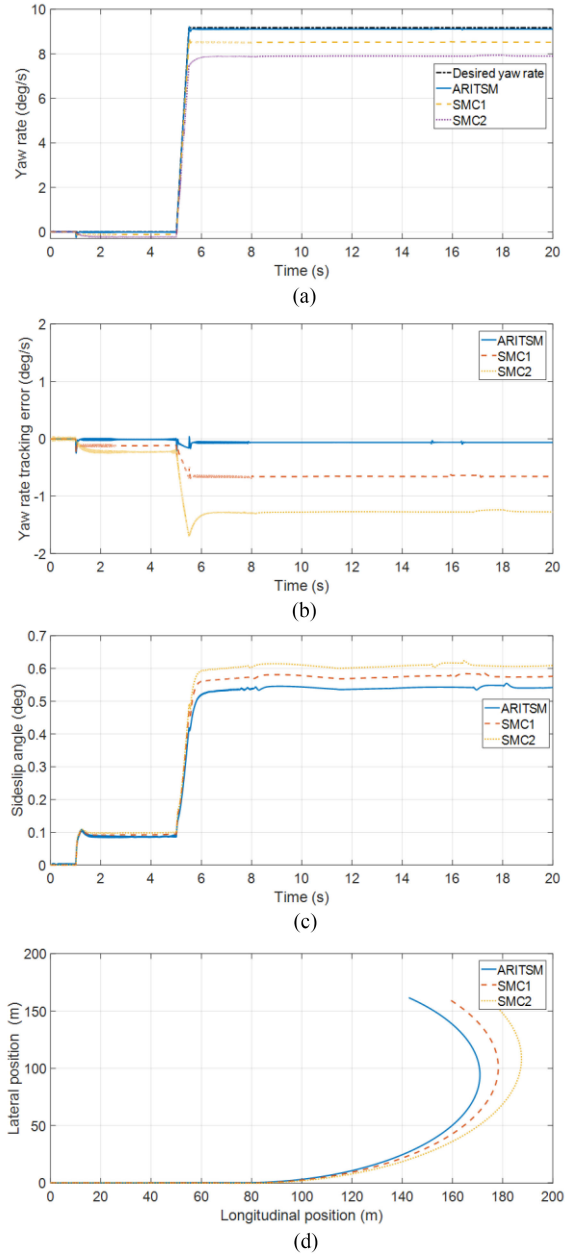

Fig. 7. Control performance of all controllers in J-turn maneuver with side wind disturbance. (a) The response curves of yaw rate. (b) The yaw rate tracking error. (c) The response curves of sideslip angle. (d) The vehicle trajectory.

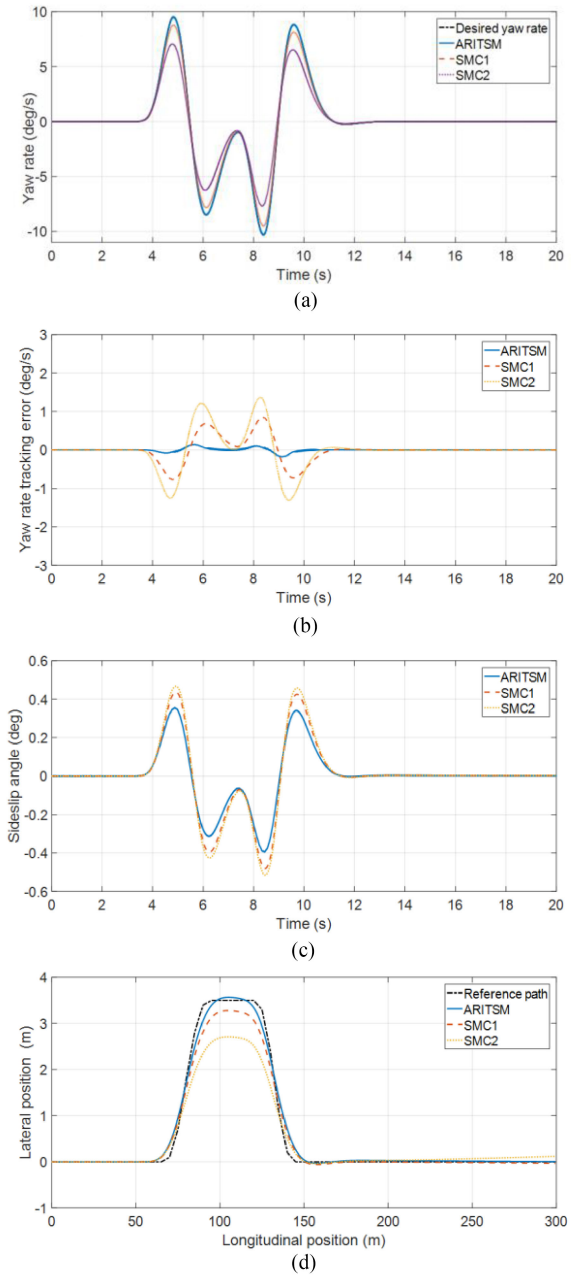

Fig. 8. Control performance of all controllers in double-lane change maneuver without side wind disturbance. (a) The response curves of yaw rate. (b) The yaw rate tracking error. (c) The response curves of sideslip angle. (d) The vehicle trajectory.

comparing Fig. 6 (a), (b) (d) with Fig. 7 (a) (b) (d), the proposed controller still exhibits the best robustness and excellence among all the controllers in tracking the desired yaw rate and obtaining the ideal trajectory. Although Fig. 6 (c) and Fig. 7(c) demonstrate that the vehicle sideslip angle is a bit larger compared with the one without disturbance for three controllers, the value is also small enough to guarantee the vehicle yaw stability.

B. Double-Lane Change Maneuver With/Without Side Wind Disturbance

Fig. 8 displays the simulation results of double-lane change maneuver without sidewind disturbance under different control methods. It is noted from Fig. 8 (a) and (b) that the ARITSM control exhibits the best tracking performance and smallest MYRE value of only 0.109 deg/s. Comparatively, the SMC1 behaves with a better tracking performance than the SMC2, with their MYRE values of 0.812 deg/s and 1.324 deg/s, respectively. In addition, Fig. 8 (c) shows that the sideslip angles are in the range of -0.5 deg to 0.5 deg under all control strategies, which is small enough to enable the driver to obtain better driving experience. It can be observed from Fig. 8(d) that, the proposed control is capable of driving the vehicle to closely track the desired trajectory and travel along the specified path.

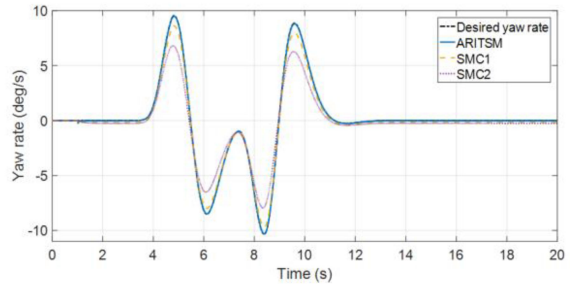

(a)

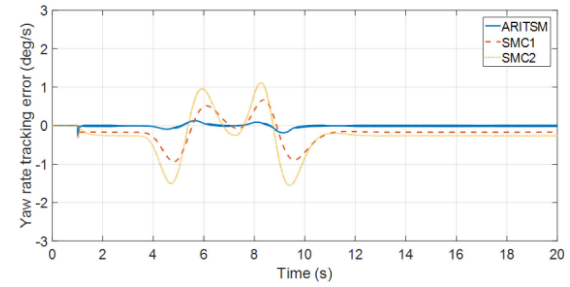

(b)

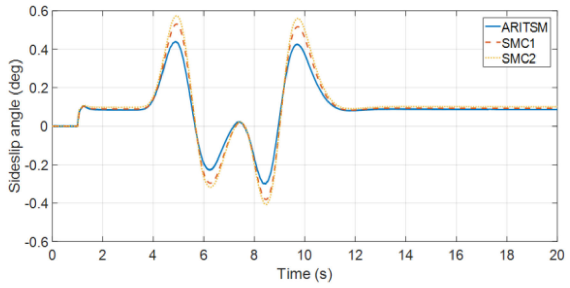

(c)

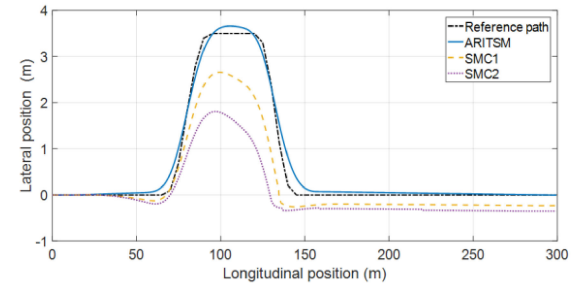

(d)

Fig. 9. Control performance of all controllers in double-lane change maneuver with side wind disturbance. (a) The response curves of yaw rate. (b) The yaw rate tracking error. (c) The response curves of sideslip angle. (d) The vehicle trajectory.

Further, simulation results with the same double-lane change maneuver under sidewind disturbance are shown in Fig. 9. It is seen that although the sideslip angles with all controllers have the similar range of values, the proposed control can ensure the yaw rate to well track the desired value, regardless of the effect of the side wind disturbance. As clearly seen from Fig. 9 (a) and (b), the vehicle with the SMC2 cannot track the desired yaw rate accurately to guarantee the vehicle yaw stability. In addition, the best vehicle trajectory is also nicely obtained by using the proposed control, as clearly demonstrated in Fig. 9(d).

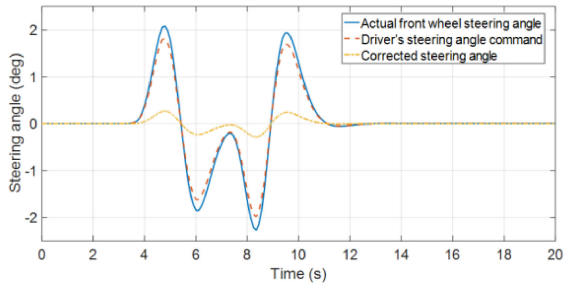

(a)

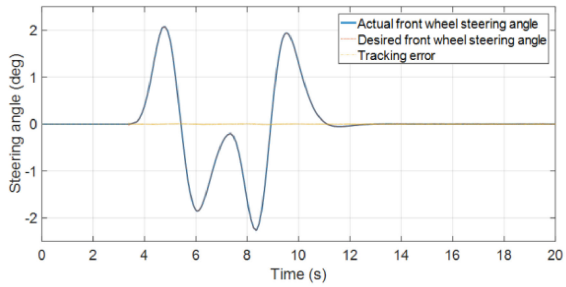

(b)

Fig. 10. Steering angle tracking performance.

TABLE V
PERFORMANCE EVALUATION UNDER DIFFERENT RANDOM INTERVALS OF PARAMETERS

Input intervals of $\boldsymbol{w}_i$ ($c_i \in [0,1]$)	Root mean square error	Input intervals of c_i ($\boldsymbol{w}_i \in [-1.1]$)	Root mean square error
$[-0.5,0.5]$	0.0094	$[0,0.5]$	0.0095
$[-1,1]$	0.0094	$[0,1]$	0.0094
$[-2,2]$	0.0090	$[0,2]$	0.0087
$[-3,3]$	0.0089	$[0,3]$	0.0085
$[-4,4]$	0.0087	$[0,4]$	0.0082

In addition, we further present the steering tracking performance of the proposed lower controller under the double-lane change maneuver as shown in Fig. 10, which verifies that the proposed lower controller obtains excellent steering performance. It is seen from Fig. 10 (a) that the steering operation of the driver is corrected by using the upper controller to improve the yaw stability and maneuverability. Since the desired front wheel steering angle of the lower controller is generated from the upper controller, the tracking performance of the lower controller can also affect the yaw control performance. Thus, the lower controller also plays an important role in the stability control system. It is clearly seen from Fig. 10 (b) that, the proposed FNTSM-based lower controller can obtain high precision steering performance with the steering tracking error of only 0.05 deg, such that the demand of stability control performance of the SbW vehicle can be well satisfied.

In order to show the sensitivity of the proposed ELM estimator in the proposed control scheme, different random input intervals are applied to double-lane change maneuver. Performance evaluation under different random intervals of parameters is listed in Table V. It is clearly observed that similar results are obtained for different random input intervals, and thus the proposed

controller will not be affected by the arbitrary input weights and the hidden layer biases.

V. Conclusion

In this paper, a novel AFS-based ESC strategy including the ARITSM controller (upper controller) and the FNTSM controller based on the ELM estimator (lower controller) has been proposed for SbW vehicles to improve the yaw stability and maneuverability. By using the terminal sliding mode technique in both upper and lower controllers, the proposed control not only ensures the yaw rate and the sideslip angle track their desired values, but also assist the vehicle to obtain the best trajectory tracking performance regardless of the external side wind disturbance. Furthermore, since the equivalent control of the lower FNTSM controller has been estimated by the developed ELM estimator, the dependence of the SbW system dynamics on the lower controller can be alleviated, which nicely guarantee the excellent tracking performance of the front steering angle for the SbW vehicle. The simulation results via Carsim and Matlab have successfully shown the superiority of the proposed control under practical steering maneuvers and sidewind disturbance. The future work on designing a sliding mode-based vehicle stability control scheme for SbW vehicles with prescribed performance by considering the rollover prevention and input saturation are under the authors' investigation.

References

[1] E. D. of China Journal of Highway and Transport, "Review on China's automotive engineering research progress: 2017," *China J. Highw. Transp.*, vol. 30, no. 6, pp. 1–197, 2017.

[2] W. Cho, J. Yoon, S. Yim, B. Koo, and K. Yi, "Estimation of tire forces for application to vehicle stability control," *IEEE Trans. Veh. Technol.*, vol. 59, no. 2, pp. 638–649, Feb. 2010.

[3] R. Rajamani, *Vehicle Dynamics and Control*. New York; Berlin, Germany: Springer Science & Business Media, 2011.

[4] P. Khatun, C. M. Bingham, N. Schofield, and P. H. Mellor, "Application of fuzzy control algorithms for electric vehicle antilock braking/traction control systems," *IEEE Trans. Veh. Technol.*, vol. 52, no. 5, pp. 1356–1364, Sep. 2003.

[5] C. Mi, H. Lin, and Y. Zhang, "Iterative learning control of antilock braking of electric and hybrid vehicles," *IEEE Trans. Veh. Technol.*, vol. 54, no. 2, pp. 486–494, Mar. 2005.

[6] L. Li, Y. Lu, R. Wang, and J. Chen, "A three-dimensional dynamics control framework of vehicle lateral stability and rollover prevention via active braking with MPC," *IEEE Trans. Ind. Electron.*, vol. 64, no. 4, pp. 3389–3401, Apr. 2017.

[7] T. Shim, S. Chang, and S. Lee, "Investigation of sliding-surface design on the performance of sliding mode controller in antilock braking systems," *IEEE Trans. Veh. Technol.*, vol. 57, no. 2, pp. 747–759, Mar. 2008.

[8] F. Tahami, S. Farhangi, and R. Kazemi, "A fuzzy logic direct yaw-moment control system for all-wheel-drive electric vehicles," *Veh. Syst. Dyn.*, vol. 41, no. 3, pp. 203–221, 2004.

[9] X. Ji, X. He, C. Lv, Y. Liu, and J. Wu, "A vehicle stability control strategy with adaptive neural network sliding mode theory based on system uncertainty approximation," *Veh. Syst. Dyn.*, vol. 56, no. 6, pp. 923–946, 2018.

[10] X. He, L. Yulong, C. Lv, X. Ji, and Y. Liu, "Emergency steering control of autonomous vehicle for collision avoidance and stabilisation," *Veh. Syst. Dyn.*, vol. 57, no. 8, pp. 1163–1187, 2018.

[11] N. Hamzah, M. K. Aripin, Y. M. Sam, H. Selamat, and M. F. Ismail, "Yaw stability improvement for four-wheel active steering vehicle using sliding mode control," in *Proc. IEEE 8th Int. Colloq. Signal Process. Appl.*, 2012, pp. 127–132.

[12] H. Zhang and J. Wang, "Vehicle lateral dynamics control through AFS/DYC and robust gain-scheduling approach," *IEEE Trans. Veh. Technol.*, vol. 65, no. 1, pp. 489–494, Jan. 2016.

[13] X. Yang, Z. Wang, and W. Peng, "Coordinated control of AFS and DYC for vehicle handling and stability based on optimal guaranteed cost theory," *Veh. Syst. Dyn.*, vol. 47, no. 1, pp. 57–79, 2009.

[14] X. Ma, P. K. Wong, J. Zhao, and Z. Xie, "Cornering stability control for vehicles with active front steering system using T-S fuzzy based sliding mode control strategy," *Mech. Syst. Signal Process.*, vol. 125, pp. 347–364, 2019.

[15] X. Ji *et al.*, "Interactive control paradigm-based robust lateral stability controller design for autonomous automobile path tracking with uncertain disturbance: A dynamic game approach," *IEEE Trans. Veh. Technol.*, vol. 67, no. 8, pp. 6906–6920, Aug. 2018.

[16] W. Huang, P. - K. Wong, K. I. Wong, C. - M. Vong, and J. Zhao, "Adaptive neural control of vehicle yaw stability with active front steering using an improved random projection neural network," *Veh. Syst. Dyn.*, to be published, doi: 10.1080/00423114.2019.1690152.

[17] H. Ohara and T. Murakami, "A stability control by active angle control of front-wheel in a vehicle system," *IEEE Trans. Ind. Electron.*, vol. 55, no. 3, pp. 1277–1285, Mar. 2008.

[18] L. Shi, H. Wang, Y. Huang, X. Jin, and S. Yang, "A novel integral terminal sliding mode control of yaw stability for steer-by-wire vehicles," in *Proc. 37th Chin. Control Conf.*, 2018, pp. 7787–7792.

[19] Y. Yamaguchi and T. Murakami, "Adaptive control for virtual steering characteristics on electric vehicle using steer-by-wire system," *IEEE Trans. Ind. Electron.*, vol. 56, no. 5, pp. 1585–1594, May 2009.

[20] P. Setlur, J. R. Wagner, D. M. Dawson, and D. Braganza, "A trajectory tracking steer-by-wire control system for ground vehicles," *IEEE Trans. Veh. Technol.*, vol. 55, no. 1, pp. 76–85, Jan. 2006.

[21] Y. Marumo and N. Katagiri, "Control effects of steer-by-wire system for motorcycles on lane-keeping performance," *Veh. Syst. Dyn.*, vol. 49, no. 8, pp. 1283–1298, 2011.

[22] H. Wang *et al.*, "Design and implementation of adaptive terminal sliding-mode control on a steer-by-wire equipped road vehicle," *IEEE Trans. Ind. Electron.*, vol. 63, no. 9, pp. 5774–5785, Sep. 2016.

[23] H. Wang, Z. Man, W. Shen, Z. Cao, J. Zheng, and J. Jin, "Robust control for steer-by-wire systems with partially known dynamics," *IEEE Trans. Ind. Informat.*, vol. 10, no. 4, pp. 2003–2015, Nov. 2014.

[24] H. Wang, Z. Man, W. Shen, and J. Zheng, "Robust sliding mode control for steer-by-wire systems with AC motors in road vehicles," in *Proc. IEEE 8th Conf. Ind. Electron. Appl.*, 2013, pp. 674–679.

[25] Z. Sun, J. Zheng, Z. Man, M. Fu, and R. Lu, "Nested adaptive super-twisting sliding mode control design for a vehicle steer-by-wire system," *Mech. Syst. Signal Process.*, vol. 122, pp. 658–672, 2019.

[26] G.-B. Huang, Q.-Y. Zhu, and C.-K. Siew, "Extreme learning machine: Theory and applications," *Neurocomputing*, vol. 70, no. 1–3, pp. 489–501, 2006.

[27] E. Grzeidak, J. A. R. Vargas, and S. C. A. Alfaro, "ELM with guaranteed performance for online approximation of dynamical systems," *Nonlinear Dyn.*, vol. 91, no. 3, pp. 1587–1603, 2018.

[28] S. Wang, W. Wang, F. Liu, Y. Tang, and X. Guan, "Identification of chaotic system using Hammerstein-ELM model," *Nonlinear Dyn.*, vol. 81, no. 3, pp. 1081–1095, 2015.

[29] M. Abe, *Vehicle Handling Dynamics: Theory and Application*. Oxford: Butterworth-Heinemann, 2015.

[30] U. Kiencke and L. Nielsen, *Automotive Control Systems: For Engine, Driveline, and Vehicle*. Berlin: Springer, 2005.

[31] S. Ding, L. Liu, and W. X. Zheng, "Sliding mode direct yaw-moment control design for in-wheel electric vehicles," *IEEE Trans. Ind. Electron.*, vol. 64, no. 8, pp. 6752–6762, Aug. 2017.

[32] K. Shao, J. Zheng, K. Huang, H. Wang, Z. Man, and M. Fu, "Finite-time control of a linear motor positioner using adaptive recursive terminal sliding mode," *IEEE Trans. Ind. Electron.*, vol. 67, no. 8, pp. 6659–6668, Aug. 2020.

[33] C. S. Chiu, "Derivative and integral terminal sliding mode control for a class of MIMO nonlinear systems," *Automatica*, vol. 48, no. 2, pp. 316–326, 2012.

[34] L. F. Y. Shtessel and C. Edwards, *Sliding Mode Control and Observation*, Series: Control Engineering. New York, NY, USA: Springer, 2016.

[35] J. Zhang *et al.*, "Adaptive sliding mode-based lateral stability control of steer-by-wire vehicles with experimental validations," *IEEE Trans. Veh. Technol.*, vol. 69, no. 9, pp. 9589–9600, Sep. 2020.

[36] B. Kwak and Y. Park, "Robust vehicle stability controller by multiple sliding mode control," in *Proc. AVEC*, 2000, pp. 41–47.

[37] L. Yang and J. Yang, "Nonsingular fast terminal sliding-mode control for nonlinear dynamical systems," *Int. J. Robust Nonlinear Control*, vol. 21, no. 16, pp. 1865–1879, 2011.

[38] H. K. Khalil and J. W. Grizzle, *Nonlinear Systems*, vol. 3. New York, NY, USA: Prentice Hall, 2002.

Jie Zhang was born in Fujian Province, China, in 1995. He received the B.S. degree in automation from the Hefei University of Technology, China, in 2018. He is currently working toward the M.S. degree in control theory and control engineering with the Hefei University of Technology, China. His research interests include sliding mode control and observer design, adaptive control, and intelligent vehicles and control.

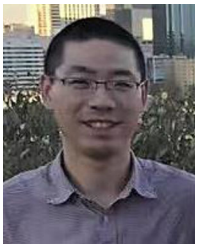

Hai Wang (Senior Member, IEEE) received the B.E. degree from Hebei Polytechnic University, China, in 2007, the M.E. degree from Guizhou University, China, in 2010, and the Ph.D. degree from the Swinburne University of Technology (SUT), Australia, in 2013, all in electrical and electronic engineering. From 2014 to 2015, he was the Postdoc Research Fellow with the Faculty of Sciences, Engineering and Technology, SUT, Australia. From 2015 to 2019, he was with the School of Electrical and Automation Engineering, Hefei University of Technology, China, where he was a Full Professor (Huangshan Young Scholar) and the Deputy Discipline Head of Automation. He is currently the Senior Lecturer with the Electrical Engineering and Academic Chair of Instrumentation and Control Engineering and Industrial Computer Systems Engineering in the Discipline of Engineering and Energy, Murdoch University, Perth, Australia. His research interests include sliding mode control and observer, adaptive control, robotics and mechatronics, neural networks, nonlinear systems, and vehicle dynamics and control. He currently serves as a Section Editor-in-Chief of Actuators, an Associate Editor for IEEE ACCESS, Lead Guest Editor of *Neural Computing & Applications*, and *Computers & Electrical Engineering*. He is also the Chair of IEEE Industrial Electronics Society Western Australia Chapter.

Mingyao Ma (Member, IEEE) received the B.Sc. and Ph.D. degrees in applied power electronics and electrical engineering from Zhejiang University, Hangzhou, China, in 2004 and 2010, respectively. In 2011, she was with the University of Central Florida, Orlando, U.S., as the Visiting Scholar. From 2012 to 2015, she joined the Newcastle University, Newcastle, U.K., as the Research Associate. From 2015, she was with the Hefei University of Technology as a Professor. Her research interests include intelligent fault diagnosis of power electronic converter, health monitoring of power device and intelligent operation and maintenance technology of photovoltaic power system.

Ming Yu received the B.E. and M.E. degrees in automobile engineering from the Hefei University of Technology, Anhui, China, in 2001 and 2004, respectively, and the Ph.D. degree in electrical and electronic engineering from Nanyang Technological University, Singapore, in 2012. From 2013 to 2014, he was a Research Fellow with the Rolls-Royce at NTU Corporate Lab, Nanyang Technological University. Since 2014, he has been with the School of Electrical and Automation Engineering, Hefei University of Technology, Hefei, China, as a Professor. His research interests include fault diagnosis and prognosis of mechatronic systems, hybrid system modeling, and evolutionary algorithms.

Amirmehdi Yazdani (Member, IEEE) received the master's degree in mechatronics and automatic control from Universiti Teknologi Malaysia, Malaysia, in 2012, and the Ph.D. degree in electrical-control engineering from Flinders University, SA, Australia, in 2017. From 2017 to 2018, he was a Postdoctoral Research Associate with Flinders University. He is currently working as a Lecturer with Electrical Engineering in the College of Science, Health, Engineering and Education, Murdoch University, WA, Australia. His areas of research interests include concerned with guidance and control of robotic, autonomous, and mechatronic systems, optimal control and state estimation theory, and intelligent control applications. He is an Academic Chair with Engineering Technology, Electrical Power Engineering, and Renewable Energy Engineering, Murdoch University. He is also the Vice-Chair of IEEE Industrial Electronic Society, WA Chapter.

Long Chen received the B.E. degree from Shan Dong University, China, in 2001, the M.E. degree from Hangzhou Dianzi University, China in 2004. He is currently a Professor with the College of Electronic Information, Hangzhou Dianzi University, China. His research interests include sliding mode control, adaptive control, robotics and mechatronics, neural networks, nonlinear systems, and EDA technology.